Assiut Univ. J. of Physics
45(1), p-p1-17(2016)

SONOCHEMICALLY SYNTHESIZED ZNO NANOSHEETS AND NANORODS: THERMAL ANNEALING EFFECTS ON THE STRUCTURE, MORPHOLOGY, OPTICAL ABSORPTION AND PHOTOLUMINESCENCE

A. A. Othman*, E. M. M. Ibrahim, M. A. Osman*, Manar A. Ali***

**Assiut University, Faculty of Science, Department of Physics, Assiut 71516, Egypt*
*** Sohag University, Faculty of Science, Department of Physics, Sohag 82524, Egypt*
**Correspondence author information*
E-mail: aaelho@yahoo.com
Tel. number: 0020882412215 - 00201011236888

Fax number: 0020882080209

Received: 29/3/2016 **Accepted:** 6/4/2016

ZnO nanopowders were successfully synthesized by ice-bath assisted sonochemical method and annealed in air for 3 h at different temperatures (T_a) range from 300 to 700 ^oC by step 100 ^oC. The effect of T_a on the structural and morphological changes was investigated by x-ray diffraction (XRD) and transmission electron microscopy (TEM). Optical properties were studied by measuring the optical absorption and photoluminescence (PL) spectra. XRD analysis showed that the thermal annealing leads to an improvement in crystallinity associated with the increase of the crystallite size, as well as the increase in both of the Zn-O bond length and unit cell volume. Also, it was found that increasing T_a results in a shift of the diffraction angle toward the lower values accompanied with the decrease of internal local strain. The morphological study confirms that the samples have a mixture of the nanosheets and nanorods structures. In addition, the length and diameter of the nanorods increase as a result of increasing T_a. The optical absorption spectra show that the exciton peak of the as-prepared sample is red shifted from 370 to 378 nm by the thermal annealing, and the optical band gap decreases from 3.45 to 3.36 eV. PL spectra were reordered at an excitation wavelength of 325 nm, and the deconvolution of the spectra reveals four emission bands; where the main UV band (at λ = 397 nm) can be attributed to exciton recombination related to near-band-edge. Furthermore, thermal annealing results in the quenching of PL intensity of the annealed samples.

***Keywords*:** ZnO, thermal annealing, nanorods, and nanosheets, photoluminescence

INTRODUCTION

Recently, many researchers focus on materials at the nanoscale due to their fascinating chemical and physical properties compared to their bulk

counterparts with large surface area and quantum confinement. Among the ZnO materials, its structure attracts more attention because of their new and unique properties which promote an achievement of high-performance materials for various applications. ZnO has also many unique properties at room temperature such as high electron mobility, high chemical and thermal stability, good transparency, direct wide optical band gap (3.3 eV), and high exciton binding energy (60 meV). These properties make ZnO vital for a wide range of applications in gas sensors [1], light emitting diodes [2], solar cells [3], UV photodetectors [4], and piezoelectric devices [5]. As a result of the multipurpose applications of zinc oxide, a number of research groups have prepared the ZnO nanostructures by various methods such as microwave assisted hydrothermal method [6], ball milling technique [7], the sonochemical process [8], and sol-gel process [9]. In the sonochemical bath, the applied high-frequency ultrasound waves generate cavities in the solution related to the acoustic cavitation phenomenon that involves formation, growth and implosive collapse of bubbles in a liquid medium, which resulting an instantaneously high temperature and pressure, which make the solvent molecules undergo hemolytic bond breakage to generate radicals. These liberated radicals lead to various chemical and physical effects in reaction pathways and mechanisms [10], [11].

Mhlongo et al. [12] prepared ZnO nanoflowers by microwave assisted hydrothermal method and annealed the sample at different temperatures (200, 600 and 900 ^{o}C) in air for 2 h. They found that the ZnO nanostructures are polycrystalline in nature with no impurity phases. The morphology changes from well-defined “flower-like” structure composed of ZnO multi-nanorods to randomly oriented “worm-like” ZnO nanostructures upon increasing the annealing temperature (T_a). Hammad et al. [13] prepared ZnO nanoparticles by the simple solution method and annealed ZnO sample at different temperatures (180, 500, 600, and 700 ^{o}C) in air for 2 h. They concluded that the particles morphology evolves from spherical to a hexagonal shape, indicating an increase in average particle size. In addition, the UV-visible and photoluminescence spectra showed a red shift when T_a was increased. Awad et al. [14] synthesized ZnO nanowires (NWs) using the thermal evaporation method with vapor–liquid–solid (VLS) growth technique. They studied the effect of annealing at high temperature up to 1673 K on the structural and compositional properties as well as the morphology of the ZnO NWs. They reported that the annealing process increases the crystallinity and the diameter of the nanowires beside that the one-dimensional NWs transform to coalesced Zero-dimensional nanoparticles. They confirm the high stability of

the Zn nanostructures at high temperature and thus the feasibility of their using as gas sensors at high temperatures.

Though a lot of literature is available on ZnO, but the effect of thermal annealing on the physical properties of ZnO nanostructures synthesized by the sonochemical technique is rarely mentioned. Therefore, in the present work, ZnO nanocrystals were synthesized by ice-bath assisted sonochemical method and annealed in air for 3 h at different T_a from 300 to 700 ^oC. Influence of thermal annealing on structural, morphological, optical, and photoluminescence properties of ZnO nanopowders was investigated.

EXPERIMENTAL DETAILS

2.1. Materials

The chemicals used for synthesizing ZnO nanocrystals were zinc acetate dihydrate [$Zn(CH_3COO)_2.2H_2O$, with purity 98% purchased from Oxford laboratory reagent], and sodium hydroxide [NaOH, with purity 96% purchased from Adwic] as starting materials, and polyethylene glycol [PEG 6000 purchased from Adwic] as surfactant agent. The absolute ethanol was purchased from Adwic.

2.2. Preparation Method

ZnO nanopowders are synthesized at room temperature via ice-bath assisted sonochemical method. In a typical method, 2 M of NaOH was dissolved in 100 ml double distilled water under magnetic stirring at 400 rpm for 5 min to form the aqueous solution A. Similarly, 0.5 M of $Zn(CH_3COO)_2.2H_2O$, and 2.5 g of PEG were dissolved in 100 ml double distilled water under magnetic stirring at 400 rpm for 5 min to form the aqueous solution B. Then, the solution A was added to solution B until the pH value of the mixture reached 12.95. The final mixture solution was sonicated with 20 KHz ultrasound waves with average output power 70 W for 1 hour. The reaction temperature was fixed at room temperature using ice-bath. The solution with a white precipitate was centrifuged and washed several times with distilled water and absolute ethanol to remove the residuals, and dried in air at 80 ºC for 18 hours. The obtained powder was annealed under air for 3 hours at different annealing temperatures in the range from 300 to 700 ^oC by step 100 ^oC.

2.3. Characterization

The crystal structure of all samples was characterized by x-ray diffraction (XRD) using the PW 1700 X-ray diffractometer with Cu-K_α radiation source λ=1.5405 Å, where the patterns were recorded at the diffraction angle (2□) range from 30^o to 70^o with step 0.06^o. The

morphological studies of the samples were carried out using a high-resolution transmission electron microscope (HRTEM) [JEOL JEM-1400 plus microscope operating at 120 kV]. Ultraviolet-visible (UV-vis) absorption spectra were recorded using Perkin-Elmer lambda 750 spectrophotometer at room temperature in the wavelength range from 300 to 800 nm. Room temperature photoluminescence (PL) emission spectra of all powder samples were measured at excitation wavelengths of 325 nm using JASCO FP-6300 spectrofluorometer.

RESULTS AND DISCUSSION

3.1. Structural Study

Fig. 1(a) shows the XRD patterns, refined by the crystal structure celref software, of the as-prepared and annealed ZnO nanostructures, synthesized by ice-bath assisted sonochemical technique. The XRD peaks are very intense confirming a high crystallinity of the samples. These peaks corresponding to (100), (002), (101), (102), (110), (103), (200), (112), and (201) planes related to the standard data of the ZnO hexagonal wurtzite structure with space group $P6_3mc$, [ICDD card no: 04-008-8198]. It is observed that no peaks corresponding to any other crystalline phase were detected in the XRD patterns of the annealed samples. Consequently, one can conclude that no effect of thermal annealing on the crystal structure of ZnO lattice was observed.

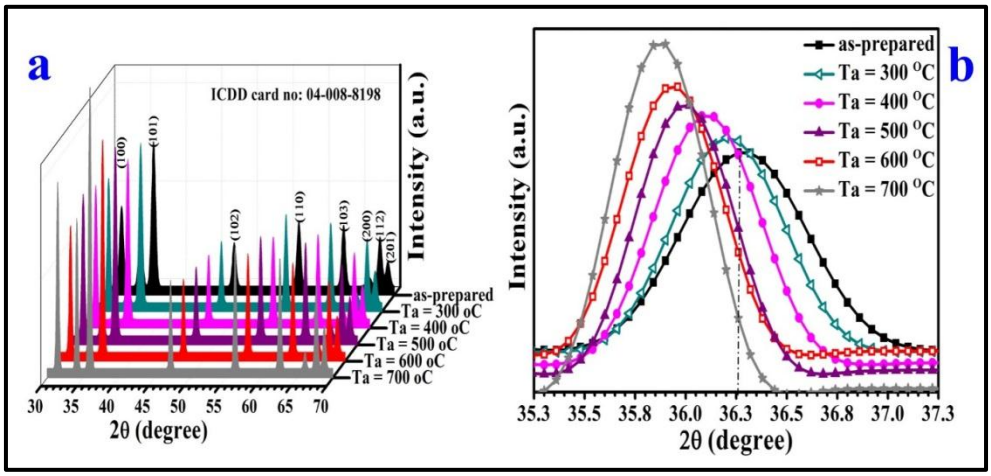

Fig. 1 (a): XRD patterns, and **(b)** the shifts of (101) diffraction peak of the as-prepared and annealed ZnO samples.

Fig. 1(b) clarifies that there are a shift for the diffraction angle (2θ) of (101) crystalline plane to lower values. An improvement of the crystallinity

(i.e. increasing the intensity) and a reduction of the full width at the half maximum was observed (FWHM) with increasing T_a.

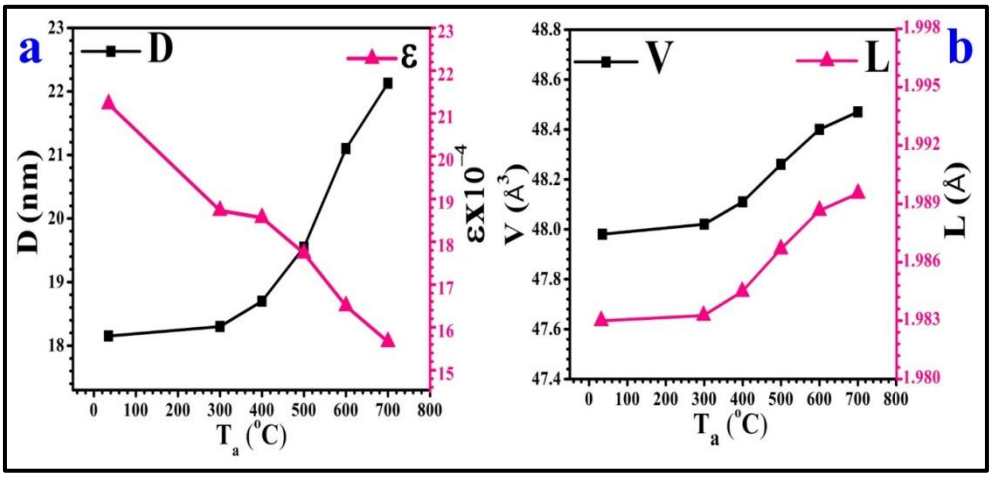

Fig. 2: Dependence of the crystallite size and microstrain on T_a **(a)**, and dependence of the unit cell volume and bond length on T_a **(b)** of the as-prepared and annealed ZnO samples**.**

These results are also associated with the increase of both Zn-O bond length and unit cell volume, as shown in Fig. 2(b). This behavior may be attributed to the reduction of the internal local strain [15], Fig. 2(a), and coalescence of nanocrystals into effectively larger crystals by thermal annealing [16]. These results agree well with Pradeev et al. [17] who reported that the unit cell volume increases while the diffraction angle shifts to lower 2Θ values with the increase in T_a. Also, Fig. 2(a) shows an increase in crystallite size from 18 to 22 nm, after the thermal annealing, associated with a reduction of the microstrain and density of grain boundaries (i.e. dislocations), as listed in Table 1. A similar increase in the crystallite size with increasing T_a was observed by Yang et al. [18], and Umar et al. [19].

The unit cell volume V for the hexagonal system was calculated using the formula [20]

$$V = 0.866\, a^2\, c \qquad (1)$$

and the Zn-O bond length L is given by [21]

$$L = \sqrt{\frac{a^2}{3} + \left(\frac{1}{2} - z\right)^2 c^2} \qquad (2)$$

where z is given by the equation

$$z = \frac{a^2}{3c^2} + \frac{1}{4} \qquad (3)$$

On the other hand, the lattice parameters *a* and *c* were calculated according to the following formula [22]

$$\frac{1}{d^2} = \frac{(h^2 + hk + k^2)}{a^2} + \frac{l^2}{c^2} \quad (4)$$

It was found that the values of the lattice parameters (a, c and c/a), see Table 1, are a good match with those in the ICDD standard reference, whereas the slight change in the lattice parameters after the thermal annealing can be attributed to the change of the crystallite size [23]. In addition, the nearly constant value of the c/a ratio confirms that the thermal annealing of ZnO nanostructures doesn't make any noticeable deformation in the lattice.

The crystallite size D_{hkl} corresponds to the most intense diffraction peak (101) was estimated using the Debye–Scherrer's formula [24]

$$D_{hkl} = \frac{0.9\lambda}{\beta_{hkl} \cos\theta} \quad (5)$$

Where λ is the wavelength of the incident x-ray beams (λ= 1.5405 Å), θ is the diffraction angle, and β_{hkl} is the FWHM corrected for the instrumental broadening of the XRD peaks?

The internal lattice strain (ε) corresponds to the (101) crystalline plane was estimated using the following relation [25]

$$\varepsilon = \frac{\beta \cos\theta}{4} \quad (6)$$

The dislocation density (δ) was calculated using [26]

$$\delta = 1/D^2 \quad (7)$$

According to Hook's law, for small dislocations in a lattice, a linear relation between the stress σ and strain is given as σ=Y ε, where Young's modulus Y (for hexagonal structure) can be represented by the following relation [27]

$$Y = \frac{\left(h^2 + \frac{(h+2k)^2}{3} + \left(\frac{al}{c}\right)^2\right)^2}{s_{11}\left(h^2 + \frac{(h+2k)^2}{3}\right) + s_{33}\left(\frac{al}{c}\right)^4 + (2s_{13} + s_{44})\left(h^2 + \frac{(h+2k)^2}{3}\right)\left(\frac{al}{c}\right)^2} \quad (8)$$

where s_{11}, s_{13}, s_{33} and s_{44} are the lattice compliances of ZnO which equal to 7.858×10^{-12}, -2.206×10^{-12}, 6.940×10^{-12}, and 23.57×10^{-12} m^2N^{-1}, respectively [28]. The energy density u (the energy per unit volume of a lattice) can be calculated from Hook's law $u = (\varepsilon^2 Y_{hkl})/2$. Values of ε, Y, σ, u, and the

above-mentioned parameters of all samples, are calculated for the crystalline plane (101) and listed in Table 1

Table 1: The diffraction angle (2θ) value, crystallite size (D), lattice parameters (a, c and c/a), unit cell volume (V), Zn-O bond length (L), internal local strain (Ɛ), dislocation density (δ), Young modulus (Y), internal stress (σ), and energy density (u) of the as-prepared and annealed ZnO samples at different annealing temperatures (T_a)

T_a (^oC)	2θ (deg.)	D (nm)	Lattice parameter			V ($Å^3$)	L (Å)	$\varepsilon x10^{-4}$	$\delta x10^{15}$ line/m^2	$Yx10^{11}$ (Pascal)	$\sigma x10^8$ (Pascal)	$ux10^5$ (J/m^3)
			a (Å)	c (Å)	c/a							
30	36.221	18.15	3.259	5.218	1.601	47.98	1.9829	21.23	3.04	1.382	2.93	3.11
300	36.148	18.30	3.259	5.219	1.601	48.02	1.9833	18.73	2.99	1.382	2.59	2.42
400	36.125	18.70	3.261	5.222	1.601	48.11	1.9845	18.56	2.86	1.382	2.56	2.38
500	36.083	19.55	3.266	5.226	1.600	48.26	1.9867	17.73	2.62	1.381	2.45	2.17
600	36.045	21.10	3.269	5.231	1.600	48.40	1.9887	16.49	2.25	1.381	2.28	1.88
700	36.000	22.13	3.269	5.237	1.602	48.47	1.9895	15.66	2.04	1.382	2.16	1.69

3.2. Morphological Study

The surface morphology of the samples under study was investigated using transmission electron microscopy (TEM). TEM images of as-prepared and annealed ZnO samples at annealing temperatures (T_a) of 400 and 700 ^oC, Fig. 3, reveal that the samples exhibit mixture of nanosheets and nanorods. The ultrasonically induced formation mechanism of ZnO nanostructures in the sonochemical bath can be expressed, according to the previous work of Mishra et al. [10], as in the following equations:

$$H_2O \leftrightarrow H^+ + OH^- \quad (9)$$

$$NaOH \leftrightarrow Na^+ + OH^- \quad (10)$$

$$Zn(CH_3COO)_2 \leftrightarrow Zn^{2+} + 2\ CH_3COO^{2-} \quad (11)$$

$$Zn^{2+} + 4\ OH^- \leftrightarrow [Zn(OH)_4]^{2-} \quad (12)$$

$$2\ [Zn(OH)_4]^{2-} \leftrightarrow 2\ ZnO + 4\ H_2 \uparrow + O_2 \uparrow \quad (13)$$

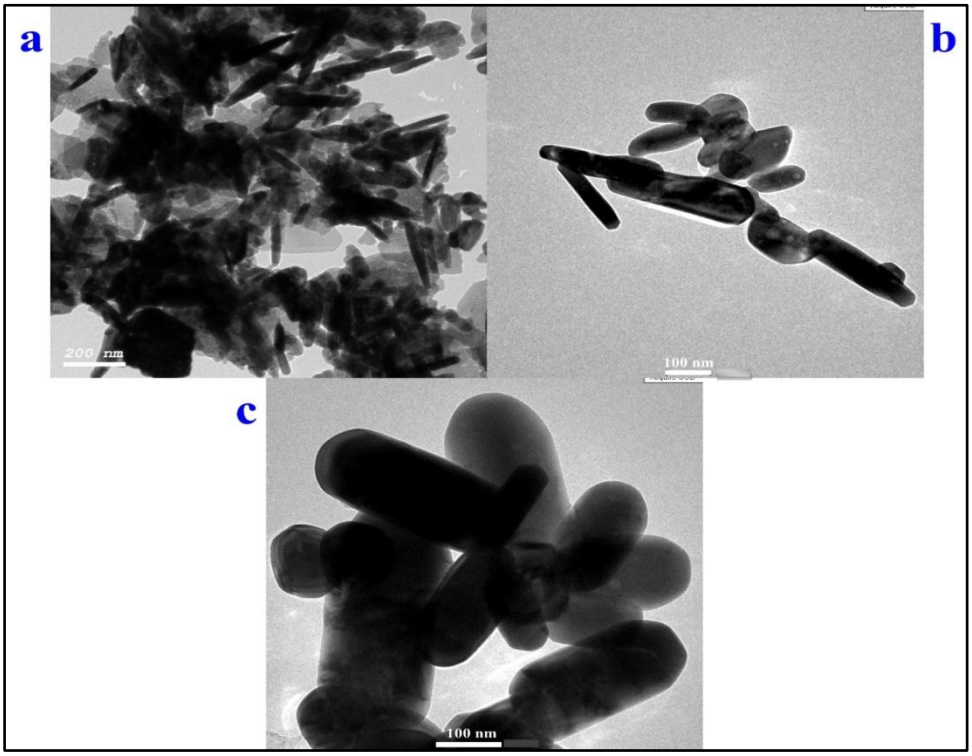

Fig. 3: TEM image of **(a)** the as-prepared sample, **(b)** the sample annealed at 400 ^{o}C, and **(c)** the sample annealed at 700 ^{o}C

Furthermore, the obtained morphology (i.e. nanorods) can be ascribed to the addition of polyethylene glycol (PEG) during the preparation of ZnO by the sonochemical method as follow:

$$\text{PEG} + \text{ZnO (nuclei)} \xrightarrow{\text{Sonication (70 Watt, 1h, 30 } ^{o}\text{C)}} \text{ZnO (nanorods)} \qquad (14)$$

Analysis of the TEM image of the as-prepared ZnO sample, Fig. 3(a), shows that the nanorods having a length in the range between 61-279 nm and diameter range between 21-51 nm. At T_a = 400 ^{o}C, Fig. 3(b), the induced lattice expansion by thermal annealing results in an increase of the nanorods length in the range 125-325 nm, and diameter in the range 40-98 nm. In addition, further, increase in T_a up to 700 ^{o}C, Fig. 3(c), leads to more lattice expansion, and the length and diameter of nanorods become in the range 181-432 and 61-181 nm, respectively. Also, thermal annealing increases the extent of agglomeration of the ZnO particles [29]. This behavior agrees well with the above-mentioned increase of the crystallite size as shown in the XRD section. Similar behavior was reported by Umar et al. [19].

3.3. Optical Absorption Behavior Study

Fig. 4(a) shows the optical absorption spectra of the as-prepared and annealed ZnO samples at different annealing temperatures (T_a). The absorption spectrum of the as-prepared sample shows strong exciton peak at 370 nm, where the corresponding exciton energy (E_{ex}) was calculated from the following formula [30]

$$E_{ex} = hC/\lambda_{max} \quad (15)$$

where h is Planck's constant, C is the velocity of light, and λ_{max} is the exciton peak wavelength.

It is shown that the thermal annealing leads to a red shift of both of the exciton peak, and the corresponding exciton energy of the as-prepared sample. The optical band gap (E_g^{opt}) values of the as-prepared and annealed samples were determined using the first derivative of the absorbance spectra with respect to photon energy, Fig. 4(b); where the maximum in the derivative of absorbance at the lower energy sites represent the exact value of E_g^{opt} [31]. It is observed that the values of E_g^{opt} of the annealed samples decreases with increasing T_a. The noticeable reduction in E_g^{opt} and E_{ex}, Fig. 4(c), can be ascribed to the reduction in internal strain accompanied with the increase in the crystallites size, Fig. 2(a), due to the improvement of crystallinity by thermal annealing [32-33].

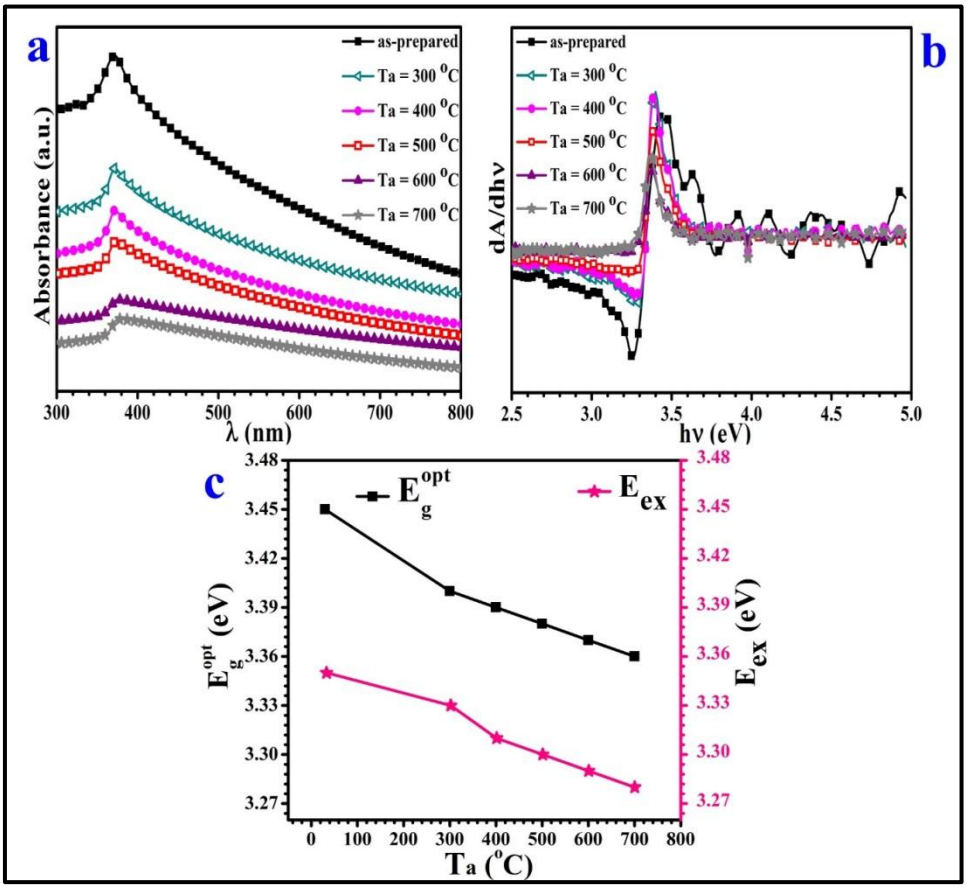

Fig. 4: (a) UV-vis absorption spectra, (b) the first derivative of absorbance of as-prepared and the ZnO samples annealed at different annealing temperature, and (c) the dependence of the optical band gap (E_g^{opt}) and exciton energy (E_{ex}) on the annealing temperature

3.4. Photoluminescence Study

Photoluminescence (PL) studies are interesting because of the valuable information gained on the quality of the crystal structure and the presence of structural defects through an identification of the various trapping and recombination levels of photo-generated carriers. Investigation of the effect of thermal annealing at different annealing temperature (T_a) on the PL spectrum of ZnO nanorods and nanosheets, PL spectra of the as-prepared and annealed ZnO samples were carried out at the excitation wavelength (λ_{ex}) of 325 nm.

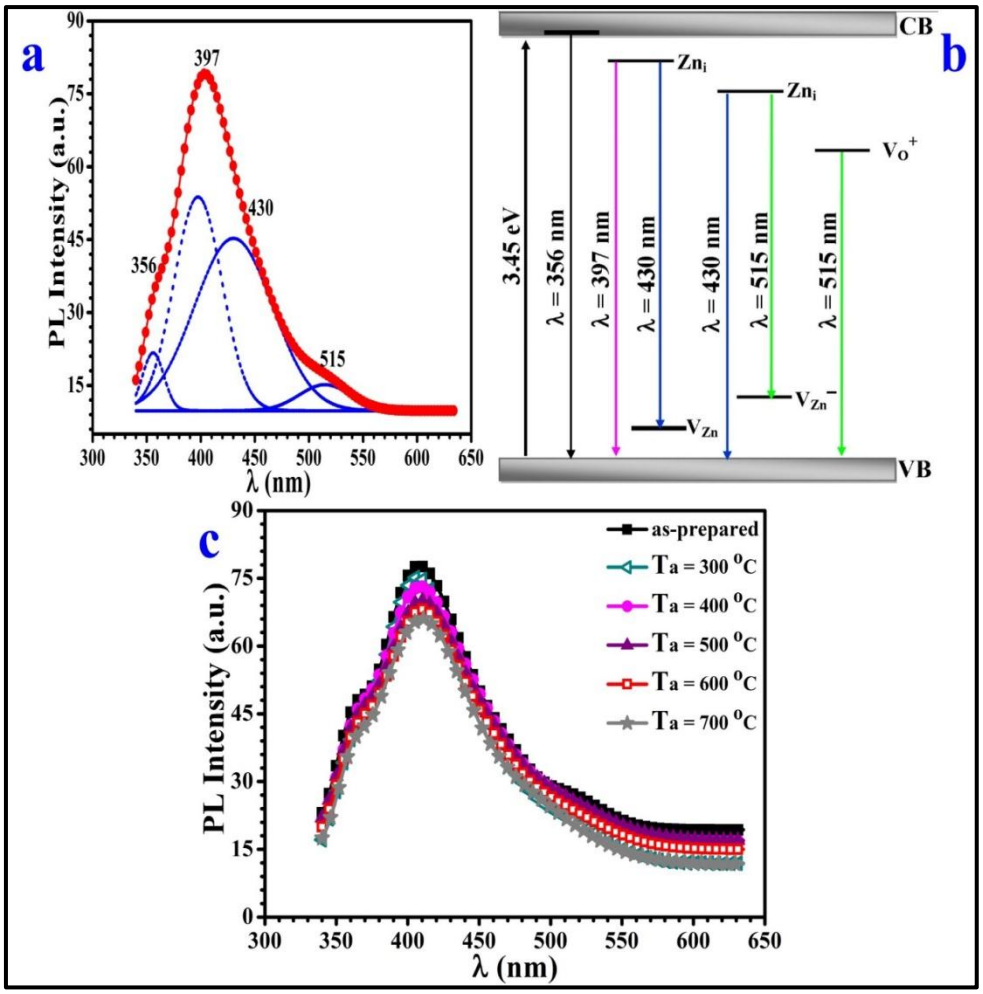

Fig. 5: (a) Normalized PL spectrum of the as-prepared ZnO sample, (b) energy band diagram, and (c) effect of T_a on the PL intensity at λ_{ex} = 325 nm

Fig. 5(a) shows normalized PL spectrum of the as-prepared ZnO nanopowders at λ_{ex}=325 nm. Gaussian fitting reveals the presence of four emission bands at 356, 397, 430, and 515 nm; hence, an energy band diagram was proposed, Fig. 5(b), in order to assign the trapping and recombination centers in the studied samples. The weak UV emission band at 356 nm (3.49 eV) may be attributed to the band to band radiative transition. The strong UV emission band centered at 397 nm (3.13 eV) may be attributed to exciton recombination related to near-band-edge (NBE) emission of photo-generated carriers [34], or to recombination of trapped electrons at shallow levels of zinc interstitial (Zn_i) with photogenerated holes [35]. The blue emission band at 430 nm (2.89 eV) can be assigned to the recombination process of trapped electrons at shallow levels of Zn_i with trapped holes at zinc vacancy (V_{Zn}),

which is consistent with the blue emission reported at 437 nm by Bylander et al. [35]. Similar blue emission band was observed by Zeng et al. [36] at 440 nm, who attributed this band to the recombination of trapped electrons at extended levels of Zn_i with photo-generated holes. The green emission band centered at 515 nm (2.41 eV) may be ascribed to either the recombination of trapped electrons at deep singly ionized oxygen vacancy (V_O^+) with photo-generated holes [37], or the recombination of trapped electron at the deep donor level of Zn_i with trapped holes at singly ionized zinc vacancies (V_{Zn}^-) acceptor levels [38]. Fig. 5(c) shows the influence of the thermal annealing on the PL spectra of ZnO samples at λ_{ex} = 325 nm. It is observed that the positions of the emission bands don't change, as well as the PL intensity decreases with the increase in T_a. This behavior of the annealed samples due to the reduction of the radiative recombination centers such as zinc and oxygen vacancies and interstitials in ZnO [39]. Similar quenching in PL intensity as a result of thermal annealing process was reported by Mhlongo et al. [12].

CONCLUSION

ZnO nanostructure has been synthesized by ice-bath assisted sonochemical technique. The dependence of the structural, morphological, optical, and photoluminescence properties on annealing temperature (T_a) has been investigated. The XRD study reveals the hexagonal wurtzite structure of ZnO. TEM images of the as-prepared and annealed samples confirm the formation of mixed nanosheets and nanorods. Increasing the T_a leads to an increase in both of the length and diameter of the nanorod due to the enhanced agglomeration of the particles. Annealing process has a significant influence on the structure properties of the samples, where The crystallite size, Zn-O bond length, and unit cell volume increase, while the diffraction angle and microstrain decrease, as a result of increasing T_a, which can be attributed to the sintering of nanocrystals into effectively larger crystals by thermal annealing. The optical absorption behavior shows that an increase in T_a results in a red shift of the excitonic peak, and decrease in the optical band gap and the corresponding exciton energy due to an improvement of the crystallinity associated with the increase of the crystallite size. Analysis of PL spectra showed that the main emission band in UV region at 397 nm, can be attributed to exciton recombination related to near-band-edge. In addition, the increase in T_a leads to the quenching of the PL intensity of the annealed samples due to the decrease of the radiative recombination centers.

REFERENCES

[1] M. Suchea, S. Christoulakis, K. Moschovis, N. Katsarakis, and G. Kiriakidis, "ZnO transparent thin films for gas sensor applications," *Thin Solid Films*, vol. 515, no. 2, pp. 551–554, Oct. 2006.

[2] H. Alvi, *Luminescence Properties of ZnO Nanostructures and Their Implementation as White Light Emitting Diodes (LEDs) Naveed ul Hassan Alvi*, no. 1378. 2011.

[3] P. Periyat and S. G. Ullattil, "Sol–gel derived nanocrystalline ZnO photoanode film for dye sensitized solar cells," *Mater. Sci. Semicond. Process.*, vol. 31, pp. 139–146, Mar. 2015.

[4] J. H. Jun, H. Seong, K. Cho, B.-M. Moon, and S. Kim, "Ultraviolet photodetectors based on ZnO nanoparticles," *Ceram. Int.*, vol. 35, no. 7, pp. 2797–2801, Sep. 2009.

[5] Z. L. Wang and J. Song, "Piezoelectric nanogenerators based on zinc oxide nanowire arrays.," *Science*, vol. 312, no. 5771, pp. 242–246, 2006.

[6] S. Liang, L. Zhu, G. Gai, Y. Yao, J. Huang, X. Ji, X. Zhou, D. Zhang, and P. Zhang, "Synthesis of morphology-controlled ZnO microstructures via a microwave-assisted hydrothermal method and their gas-sensing property.," *Ultrason. Sonochem.*, vol. 21, no. 4, pp. 1335–42, 2014.

[7] P. K. Giri, S. Bhattacharyya, D. K. Singh, R. Kesavamoorthy, B. K. Panigrahi, and K. G. M. Nair, "Correlation between microstructure and optical properties of ZnO nanoparticles synthesized by ball milling," *J. Appl. Phys.*, vol. 102, no. 9, p. 93515, 2007.

[8] A. K. Zak, W. H. Majid, H. Z. Wang, R. Yousefi, A. M. Golsheikh, and Z. F. Ren, "Ultrasonics Sonochemistry Sonochemical synthesis of hierarchical ZnO nanostructures," *Ultrason. - Sonochemistry*, vol. 20, no. 1, pp. 395–400, 2013.

[9] M. M. Ba-abbad, A. Amir, H. Kadhum, A. Bakar, and M. S. Takriff, "The effect of process parameters on the size of ZnO nanoparticles synthesized via the sol – gel technique," *J. Alloys Compd.*, vol. 550, pp. 63–70, 2013.

[10] R. S. Yadav, P. Mishra, and A. C. Pandey, "Growth mechanism and optical property of ZnO nanoparticles synthesized by sonochemical method," *Ultrason. Sonochem.*, vol. 15, no. 5, pp. 863–868, Jul. 2008.

[11] A. Hassanjani-Roshan, S. M. Kazemzadeh, M. R. Vaezi, and A. Shokuhfar, "The effect of sonication power on the sonochemical synthesis of titania nanoparticles," *J. Ceram. Process. Res.*, vol. 12, no. 3, pp. 299–303, 2011.

[12] G. H. Mhlongo, D. E. Motaung, S. S. Nkosi, H. C. Swart, G. F. Malgas, K. T. Hillie, and B. W. Mwakikunga, "Applied Surface Science Temperature-dependence on the structural , optical , and

paramagnetic properties of ZnO nanostructures," *Appl. Surf. Sci.*, vol. 293, pp. 62–70, 2014.

[13] T. M. Hammad, J. K. Salem, and R. G. Harrison, "The influence of annealing temperature on the structure, morphologies and optical properties of ZnO nanoparticles," *Superlattices Microstruct.*, vol. 47, no. 2, pp. 335–340, 2010.

[14] M. A. Awad, E. M. M. Ibrahim, and A. M. Ahmed, "Synthesis and thermal stability of ZnO nanowires," *J. Therm. Anal. Calorim.*, vol. 117, no. 2, pp. 635–642, 2014.

[15] J. P. Mathew, G. Varghese, and J. Mathew, "Effect of post-thermal annealing on the structural and optical properties of ZnO thin films prepared from a polymer precursor," *Chinese Phys. B*, vol. 21, no. 7, p. 78104, 2012.

[16] R. B. Kale and C. D. Lokhande, "Room temperature deposition of ZnSe thin films by successive ionic layer adsorption and reaction (SILAR) method," *Mater. Res. Bull.*, vol. 39, no. 12, pp. 1829–1839, 2004.

[17] K. Sadayandi, "Effect of temperature on structural, optical and photoluminescence studies on ZnO nanoparticles synthesized by the standard co-precipitation method," *Phys. B Condens. Matter*, vol. 487, no. 1, pp. 1–7, 2016.

[18] J. Yang, X. Liu, L. Yang, Y. Wang, Y. Zhang, J. Lang, M. Gao, and B. Feng, "Effect of annealing temperature on the structure and optical properties of ZnO nanoparticles," *J. Alloys Compd.*, vol. 477, no. 1–2, pp. 632–635, 2009.

[19] A. Umar, R. Kumar, G. Kumar, H. Algarni, and S. H. Kim, "Effect of annealing temperature on the properties and photocatalytic efficiencies of ZnO nanoparticles," *J. Alloys Compd.*, vol. 648, pp. 46–52, 2015.

[20] S. Singhal, J. Kaur, T. Namgyal, and R. Sharma, "Cu-doped ZnO nanoparticles: Synthesis, structural and electrical properties," *Phys. B Condens. Matter*, vol. 407, no. 8, pp. 1223–1226, Apr. 2012.

[21] G. Srinivasan, R. T. Rajendra Kumar, and J. Kumar, "Li doped and undoped ZnO nanocrystalline thin films: a comparative study of structural and optical properties," *J. Sol-Gel Sci. Technol.*, vol. 43, no. 2, pp. 171–177, May 2007.

[22] A. K. Zak, W. H. A. Majid, M. E. Abrishami, and R. Youse, "X-ray analysis of ZnO nanoparticles by Williamson e Hall and size e strain plot methods," vol. 13, 2011.

[23] K. Nogi, M. Naito, and T. Yokoyama, *Nanoparticle technology handbook*. Elsevier, 2012.

[24] K. K. Nanda and S. N. Sahu, "One-Dimensional Quantum Confinement in Electrodeposited PbS Nanocrystalline Semiconductors," *Adv. Mater.*, vol. 13, no. 4, pp. 280–283, 2001.

[25] W. D. Callister and D. G. Rethwisch, *Materials science and engineering: an introduction*, vol. 7. Wiley New York, 2007.
[26] K. Raja, P. S. Ramesh, and D. Geetha, "Synthesis, structural and optical properties of ZnO and Ni-doped ZnO hexagonal nanorods by Co-precipitation method," *Spectrochim. Acta - Part A Mol. Biomol. Spectrosc.*, vol. 120, pp. 19–24, 2014.
[27] J.-M. Zhang, Y. Zhang, K.-W. Xu, and V. Ji, "General compliance transformation relation and applications for anisotropic hexagonal metals," *Solid State Commun.*, vol. 139, no. 3, pp. 87–91, Jul. 2006.
[28] C.-Y. Chen, M. Wang, J.-Y. Li, N. Pootrakulchote, L. Alibabaei, C. Ngoc-le, J.-D. Decoppet, J.-H. Tsai, C. Grätzel, C.-G. Wu, S. M. Zakeeruddin, and M. Grätzel, "Highly Efficient Light-Harvesting Ruthenium Sensitizer for Thin-Film Dye-Sensitized Solar Cells," *ACS Nano*, vol. 3, no. 10, pp. 3103–3109, Sep. 2009.
[29] O. Mekasuwandumrong, P. Pawinrat, P. Praserthdam, and J. Panpranot, "Effects of synthesis conditions and annealing post-treatment on the photocatalytic activities of ZnO nanoparticles in the degradation of methylene blue dye," *Chem. Eng. J.*, vol. 164, no. 1, pp. 77–84, 2010.
[30] S. Dutta, S. Chattopadhyay, D. Jana, a. Banerjee, S. Manik, S. K. Pradhan, M. Sutradhar, and a. Sarkar, "Annealing effect on nano-ZnO powder studied from positron lifetime and optical absorption spectroscopy," *J. Appl. Phys.*, vol. 100, no. 11, p. 114328, 2006.
[31] A. K. Zak, M. E. Abrishami, W. H. A. Majid, R. Yousefi, and S. M. Hosseini, "Effects of annealing temperature on some structural and optical properties of ZnO nanoparticles prepared by a modified sol–gel combustion method," *Ceram. Int.*, vol. 37, no. 1, pp. 393–398, 2011.
[32] S. Kumar and P. D. Sahare, "Effects of Annealing on the Surface Defects of Zinc Oxide Nanoparticles," *Nano*, vol. 07, no. 03, p. 1250022, Jun. 2012.
[33] C. Sui, Z. Lu, and T. Xu, "Effects of annealing temperature on photoluminescence of ZnO nanorods hydrothermally grown on a ZnO:Al seed layer," *Opt. Mater. (Amst).*, vol. 35, no. 12, pp. 2649–2653, 2013.
[34] M. Mazhdi, J. Saydi, M. Karimi, J. Seidi, and F. Mazhdi, "Optik A study on optical , photoluminescence and thermoluminescence properties of ZnO and Mn doped-ZnO nanocrystalline particles," *Opt. - Int. J. Light Electron Opt.*, vol. 124, no. 20, pp. 4128–4133, Oct. 2013.
[35] E. G. Bylander, "Surface effects on the low-energy cathodoluminescence of zinc oxide," *J. Appl. Phys.*, vol. 49, no. 3, pp. 1188–1195, 1978.
[36] H. Zeng, G. Duan, Y. Li, S. Yang, X. Xu, and W. Cai, "Blue

luminescence of ZnO nanoparticles based on non-equilibrium processes: defect origins and emission controls," *Adv. Funct. Mater.*, vol. 20, no. 4, pp. 561–572, 2010.

[37] K. Vanheusden, W. L. Warren, C. H. Seager, D. R. Tallant, J. a Voigt, and B. E. Gnade, "Mechanisms behind green photoluminescence in ZnO phosphor powders," *J. Appl. Phys.*, vol. 79, no. 10, pp. 7983–7990, 1996.

[38] N. Y. Garces, L. Wang, L. Bai, N. C. Giles, L. E. Halliburton, and G. Cantwell, "Role of copper in the green luminescence from ZnO crystals," *Appl. Phys. Lett.*, vol. 81, no. 4, pp. 622–624, 2002.

[39] S. K. Panda, S. Chakrabarti, B. Satpati, P. V Satyam, and S. Chaudhuri, "Optical and microstructural characterization of CdS – ZnO nanocomposite thin films prepared by sol – gel technique," vol. 37, pp. 628–633, 2004.

رقائق وقضبان نانومترية من أكسيد الزنك المحضرة بطريقة الموجات فوق الصوتية: تأثير التخمير الحرارى على التركيب و المورفولوجى والأمتصاص الضوئى والتألق الوميض

على عبد الحميد عثمان*- إسلام محمد محمد إبراهيم- محمد عبد الحميد عثمان*- منار عبد الرحمن على***

قسم الفيزياء- كلية العلوم- جامعة أسيوط

***** قسم الفيزياء- كلية العلوم- جامعة سوهاج***

تم تحضير مركب أكسيد الزنك النانومترى بنجاح بطريقة الموجات الفوق صوتية بمتوسط قدرة تبلغ ٧٠ وات لمدة ساعة، كما تخمير العينات فى الهواء لمدة ثلاث ساعات عند درجات حرارة مختلفة تبدأ من ٣٠٠ إلى ٧٠٠ بزيادة قدرها ١٠٠ درجة سليزيوس.

تم دراسة تأثيردرجة التخميرالحرارى على التغيرات التركيبة والشكلية الحادثة نتيجة لعملية التخمير الحرارى بواسطة حيود الأشعة السينية والميكرسكوب الألكترونى ، بالإضافة إلى دراسة سلوك أطياف الإمتصاص الضوئى وأطياف التألق الضوئى الفوتونى لعينة أكسيد الزنك. وقد وُجد من تحليل حيود الأشعة السينية أن زيادة درجة حرارة التخمير تؤدى إلى تمدد طول الرابطة وزيادة حجم البلورة وحجم وحدة بناء الخلية، بالإضافة إلى نقص الإنفعال الداخلى للشبيكة، وإزاحة زاوية الحيود إلى القيم الأقل. بينت الدراسات الشكلية للعينات المخمرة أن العينات عبارة عن خليط من القضبان والرقائق فى مدى النانومتر، حيث أظهرت الدراسة أن زيادة درجة حرارة التخمير تؤدى إلى زيادة كل من أطوال وأنصاف أقطار القضبان النانومترية نتيجة لزيادة تجمع حبيبات أكسيد الزنك. يُظهر تحليل أطياف الإمتصاص الضوئى أن زيادة درجة حرارة التخمير تؤدى بدورها إلى زيادة قمة الإكسيتون من ٣٧٠ إلى ٣٧٨ نانومتر، ونقص قيمة فجوة الطاقة الضوئية من ٣.٣٥ إلى ٣.٢٨ إلكترون فولت. أظهرت دراسة أطياف التألق الضوئى الفوتونى للعينات التى تم تخميرها أن شدة التألق الضوئى الفوتونى تقل نتيجة لنقص مراكز إعادة الإتحاد المشعة المرتبطة بنقص تركيز الشوائب السطحية الذاتية بفعل زيادة درجة التخمير الحرارى.